Supplemental Materials

Depression-related increases and decreases in appetite reveal dissociable patterns of aberrant activity in reward and interoceptive neurocircuitry

W. Kyle Simmons[1,2], Kaiping Burrows[1], Jason A. Avery[1], Kara L. Kerr[1,3], Jerzy Bodurka[1,4], Cary R. Savage[5], Wayne C. Drevets[6]

1. Laureate Institute for Brain Research, Tulsa, OK
2. Faculty of Community Medicine, The University of Tulsa, Tulsa, OK
3. Department of Psychology, The University of Tulsa, Tulsa, OK
4. College of Engineering, The University of Oklahoma, Tulsa, OK
5. Center for Health Behavior Neuroscience, Kansas University Medical Center, Kansas City, KS
6. Janssen Research & Development, LLC., of Johnson & Johnson, Inc., Titusville, NJ

SUPPLEMENTAL METHODS

Supplemental Participant Information

All subjects underwent clinical screening assessments including a Structured Clinical Interview for DSM-IV Axis I Disorders (SCID-I) performed by Master's and Doctoral-level clinicians with experience in psychiatric diagnosis and training on conducting the SCID-I. In addition, for every subject, the SCID-I results were compared to those of unstructured psychiatric interviews performed by a research psychiatrist, with any discrepancies between the two assessments resolved prior to inclusion in the study. All depressed subjects met DSM-IV criteria for current major depressive disorder.

Depression severity was assessed using the 25-item Hamilton Depression Rating Scale (HDRS). Anxiety severity was assessed using the Hamilton Anxiety Rating Scale (HARS) and the State-Trait Anxiety Inventory (STAI). The two depression groups did not differ with respect to depression severity as measured by the HDRS, anxiety severity as measured by the HARS, or state or trait anxiety as measured using the STAI (see Table 1).

Volunteers were excluded from participation if they had been exposed to psychotropic medications or other drugs likely to affect cerebral function or blood flow within three weeks (six weeks for fluoxetine), or had manifested a major neurological or medical disorder, substance abuse, a past history of traumatic brain injury, or current pregnancy. Subjects with an unhealthily low BMI < 18.5 were also excluded from the study. Additionally, healthy control subjects were excluded for having met criteria for any Axis I psychiatric disorder on the SCID-I, or had a first-degree relative with any Axis I psychiatric disorder. All subjects received compensation for their participation and provided written informed consent as approved by LIBR's Institutional Review Board of record.

Subjects were queried about the time interval between scanning and their most recent food intake. The interval did not differ between the three groups (HC Mean (SD) = 4.03 hours [1.43]; depressed-increase appetite Mean [SD] = 5.38 hours [3.48]; depressed-decrease appetite Mean (SD) = 5.97 hours [4.51], p-value of all pair-wise comparisons > .28).

Supplemental Experimental Design Information

During the Food/non-food Picture task, subjects viewed a broad selection of food and non-food photographs, including images of appetizing foods high in both fat and sugar content, as well as many healthy food options such as fruits and vegetables. The non-food photographs all depicted small, manipulable household and office implements (e.g., hammers, staplers, pliers, etc.). In total, there were 180 food and 45 non-food pictures presented. The pictures were normed in an earlier study to ensure that food and non-food picture naming accuracy was at ceiling and typicality ratings were not different (and in fact, nearly identical) between groups (1).

All photographs were presented in the scanner for 2.5 seconds each in a pseudorandom order that was optimized for fMRI by optseq2 (http://surfer.nmr.mgh.harvard.edu/optseq/). During the interstimulus intervals, a

fixation cross appeared for variable durations (range 2.5-12.5 seconds). Subjects underwent 3 scanning runs, each lasting 5 minutes and 48 seconds.

During the Food Pleasantness Rating Task, subjects saw food images for 5 seconds and provided ratings on a 1-to-7 scale in response to the following question: ‘‘If given the opportunity right now, how pleasant would it be to eat this food?’’ On the response scale, “1” was depicted as ‘‘neutral’’ and seven as ‘‘extremely pleasant’’. The pleasantness scale also included an ‘‘unpleasant’’ option represented by the letter ‘‘X’’ located below the number line. Subjects were instructed to select the ‘‘X’’ if they believed it would be unpleasant to eat the depicted food. The stimuli depicted four broad classes of food items, including high-fat high-sweet foods (e.g., primarily “dessert” foods such as cake and ice cream), high-fat low-sweet foods (e.g., savory foods such as pizza), low-fat high-sweet foods (e.g., fruits), and low-fat low-sweet foods (e.g., vegetables). The task methods and stimuli is a variant of an imaging task reported previously by our lab (2). Subjects were shown 3 different exemplars of 48 distinct classes of food items. The 144 food images depicted a variety of foods, including many high calorie processed foods (e.g., cheeseburgers, French fries, pizza, cake, cinnamon rolls, ice cream, etc.) as well as uncooked fruits and vegetables (grapes, strawberries, cauliflower, broccoli, carrots, etc.).

Supplemental Information on MRI Data Acquisition

A brain-dedicated receive-only 32-element coil array (Nova Medical Inc), optimized for parallel imaging, was used for MRI signal reception. A single-shot gradient-recalled echo-planar imaging (EPI) sequence with Sensitivity Encoding (SENSE) depicting blood oxygenation level-dependent (BOLD) contrast was used for functional scans

EPI imaging parameters for the food/non-food picture task scanning runs were as follows: FOV/slice/gap=220/2.9/0mm, axial slices per volume=44, acquisition matrix=96×96, repetition/echo time TR/TE=2500/22ms, SENSE acceleration factor R=2 in the phase encoding (anterior-posterior) direction, flip angle=70°, sampling bandwidth=250kHz, number of volumes=139, scan time=348sec. All EPI images were reconstructed into a 128×128 matrix, in which the resulting fMRI voxel volume was $1.875\times1.875\times2.9mm^3$. As demonstrated by measurements of temporal signal-to-noise ratio (TSNR), these scan parameters ensured high image quality and reduced magnetic susceptibility artifacts within limbic regions, including the OFC and ventromedial prefrontal cortex (see Figure S4). The following EPI parameters were used for the resting scans: field of view (FOV)/slice/gap = 240/2.9/0 mm, axial slices per volume = 46, acquisition matrix = 96 × 96, repetition/echo time TR/TE = 2500/25 ms, SENSE acceleration factor R = 2 in the phase encoding (anterior-posterior) direction, flip angle = 90°, sampling bandwidth = 250 kHz, number of volumes = 180, scan time = 450 sec.

To provide anatomical reference for the functional image analysis, we also collected a T1-weighted magnetization-prepared rapid gradient-echo (MPRAGE) sequence with SENSE. The anatomical scan had the following parameters: FOV=240 x 216 mm^2, axial slices per volume=176, slice thickness=0.9 mm,

image matrix=256 x 256, voxel volume 0.938 x 0.938 x 0.9 mm^3, TR/TE=5/2.02 ms, acceleration factor R=2, flip angle=8º, inversion time TI=725 ms, sampling bandwidth=31.25 kHz, scan time=373 sec.

Supplemental Information on Preprocessing and Subject-level Analyses of the Food/non-food Picture Task Imaging Data.

Functional image preprocessing was performed using AFNI (http://afni.nimh.nih.gov/afni). The anatomical scan was registered to the first volume of the resting-state EPI time-course using AFNI's anatomical-to-epi alignment procedure. The anatomical scan was then spatially transformed to the stereotaxic array of Talairach and Tournoux using AFNI's automated algorithm, saving the transformation parameters for use later in the pre-processing. The first 4 volumes were then cut from each EPI timecourse to allow the fMRI signal to reach steady state, and a slice timing correction was applied to all EPI volumes. Estimates of the transformations necessary to register all EPI volumes to the first volume of the first EPI time-course were saved. Motion correction and spatial transformation of the EPI data were implemented in a single image transformation, and all images were resampled to 1.75x1.75x1.75 mm^3 isometric voxels. The EPI data were then smoothed with a 6-mm full-width at half-maximum Gaussian kernel, and signal intensity normalized to reflect percent signal change from each voxel's mean intensity across the time-course.

Each subject's functional imaging data were analyzed using multiple linear regression. The regression model included regressors for the food and non-food object picture presentations. To adjust the model for the shape and delay of the BOLD function, task regressors were constructed by convolving a series of gamma-variate functions each beginning at the onset of the presentation of a picture stimulus. Additionally, the model included regressors of non-interest to account for each run's signal mean, linear, quadratic, and cubic signal trends, as well as the 6 normalized motion parameters (3 translations, 3 rotations) computed during the image registration preprocessing.

Supplemental Information on Preprocessing and Subject-level Analyses of Resting-State Scan Data.

Preprocessing of the resting-state scans was performed using a modified version of the ANATICOR method (3), implemented through the AFNI program afni_restproc.py. As with the task EPI data, the first 4 volumes of the resting state-scan were excluded to allow the fMRI signal to reach steady state. Following this, a de-spiking interpolation algorithm (AFNI's 3dDespike) was used to remove transient signal spikes from the EPI data that might otherwise artificially inflate correlation estimates between voxel time-series. This was then followed with a slice time correction. Each resting state EPI volume was registered to the first volume of the time course, which was itself registered to the anatomical scan. Using the high-resolution anatomical scan, masks of the subject's ventricles and white matter were constructed using FreeSurfer (http://surfer.nmr.mgh.harvard.edu/). After resampling the masks to the same resolution as the EPI scan, each mask was then eroded by a single voxel in each

direction to prevent partial volume effects that might include signal from gray matter voxels in the mask. The average time course during the resting-state scan was extracted from the ventricle mask and subsequently used to account for any components of the MR signal present in the cerebrospinal fluid in the ventricles. Next, local physiological noise present in white matter was estimated using the AFNI program 3dLocalstat, which calculated the average signal time-course for all white matter voxels within a 1.5 cm radius of each gray matter voxel. Respiration and cardiac data collected by pulse-oximetry and respiration belt recording during scanning was used to calculate RETROICOR (4) and respiration volume per time (RVT) (5) parameters using the RetroTS.m plugin for MATLAB. Additional regressors of non-interest were constructed from the mean, linear, quadratic, and cubic signal trends, as well as the 6 normalized motion parameters (3 translations, 3 rotations) computed during the image registration preprocessing. In total, the estimates of physiological and non-physiological noise included the 6 motion parameters, the average ventricle signal, the average local white matter signal, and 13 respiration regressors from RETROICOR and RVT. The predicted time-course for these nuisance variables was constructed using AFNI's 3dTfitter program and then subtracted from each resting-state voxel time-course, yielding a residual time-course for each voxel. The residual EPI time series was then smoothed with a 6 mm FWHM Gaussian kernel, resampled to a 1.75x1.75x1.75 mm^3 grid, and spatially transformed to Talairach stereotaxic space (6) for all subsequent analyses.

Regarding subject-level analyses of the resting state data, 15 depressed subjects with *increased* appetite, 15 depressed subjects with *decreased* appetite, and 13 healthy non-depressed subjects performed the resting-state scan, food/non-food picture task, and also completed the food pleasantness rating task all on the same scan day. For both healthy and depressed subjects, resting-state functional connectivity maps were separately constructed for both of the mid-insula food-responsive regions (identified in the healthy participants' food/non-food picture task imaging data; Figure 1) as follows: The AFNI program 3dmaskave was first used to extract the average time-series from the pre-processed resting-state data within each of the seed regions (defined as those regions that exhibited a greater response to food and non-food images after correction for multiple correction; see Figure 1 and Table S1). Next, separate multiple regression analyses were used to produce voxel-wise maps of the correlation coefficients between the time-course of the seed regions and all other voxels in the brain. The r-value maps made by this process were then fisher-transformed into Z-score maps, for use in the group analysis.

These resting-state functional connectivity maps were then used to identify any regions of the brain where functional connectivity to these interoceptive and food-responsive regions was modulated by the magnitude of inferred food pleasantness ratings provided by the subjects in the food pleasantness rating task. At the group level, the average ratings from the food pleasantness task were regressed against the functional connectivity maps produced from the seven seed regions, using the AFNI program 3dttest++.

Resultant maps were cluster-size corrected for multiple comparisons at $p < .05$ as described below.

Group Analyses

Group analyses were implemented using multiple strategies. Appetite changes in depression could be due to (A) differential responses between depressed groups within brain regions known to underlie normal responses to food stimuli, or (B) differential responses between depressed groups within brain regions that do not necessarily exhibit food-specific responses in healthy subjects, or (C) both. To address these possibilities we conducted the following group analyses.

With regard to (A), the human brain mapping literature has accumulated substantial evidence as to which regions exhibit differential responses to food versus non-food stimuli. Meta-analyses identify these regions as being OFC, ventromedial prefrontal cortex, striatum and ventral pallidum, anterior insula, and middle insula (7). We could identify these regions from reported studies, but we know that many factors, including age, body mass, and scanner sensitivity and spatial resolution influence the activity and spatial representation of these regions (7, 8), so it is most accurate to localize them within a group of healthy subjects that are matched to the depressed subjects on these variables under a uniform set of experimental conditions. Therefore, in the present study, we used whole-brain voxel-wise analyses to map food-responsive regions in healthy non-depressed adult participants and then interrogated the activity of these regions in groups of unmedicated depressed subjects that reported either increased or decreased appetite. Food-responsive regions in the HC sample were identified using a random-effects paired-sample t-test of the healthy subjects' beta coefficients for food and non-food stimuli derived from the subject-level regression analyses. The resulting group statistical map was corrected for multiple comparisons according to the following procedures. Based on the prior research (described above) identifying regions underlying appetitive responses to food images and in depression, structurally defined regions of interest (ROIs) were constructed. These regions included the orbitofrontal cortex (OFC), ventral striatum, caudate, putamen, amygdala, subgenual anterior cingulate (sgACC), ventral pallidum, and insula (see below for ROI anatomical definitions). After setting a voxel-wise threshold of $p < .005$, the required cluster size threshold to achieve correction at $p < .05$ within the volume of the anatomical ROI was estimated using Monte Carlo simulations in the AFNI program 3dClustSim and applied to the statistical maps. A voxelwise threshold of $p < .0005$ and cluster-size correction to $p < .05$ was utilized for brain regions outside the *a priori* hypothesized ROIs. Comparisons among the two depressed groups were next conducted as random effects, independent t-tests on the subjects' beta coefficients from the subject-level regression analyses within each of the seven corrected ROIs identified in the analyses of the HC subjects' data.

We next sought to determine whether additional regions outside of those identified in the HC subjects alone might contribute to appetite differences between depressed subjects. We therefore conducted an additional voxel-wise

one-way Analysis of Variance (ANOVA) to identify brain regions where the groups exhibited differential responses to food. The resulting ANOVA F-map was corrected for multiple comparisons according to the procedures described in the preceding paragraph. We then conducted follow-up planned comparisons using independent samples t-tests of the simple effects within each ROI to determine which group differences supported the significant ANOVA findings. Each of these post-hoc t-tests was corrected for multiple comparisons using Tukey's HSD test.

Anatomical ROI definitions

Using AFNI's TT_N27 template brain volume, the orbitofrontal cortex ROI was anatomically defined anteriorly by the frontal pole and posteriorly by a line drawn at y = 20 (stereotaxic coordinates refer to distance in mm from the anterior commissure, in the normalized space of Talairach and Tournoux, 1988). The OFC ROI extended to the ventral surface of the cortex, and the fundus of the transverse orbital sulcus (9) defined the dorsal extent. The ROI was defined medially by the lateral edge of the olfactory sulcus and laterally by the more medial of either the lateral intermediate orbital sulcus or the lateral orbital sulcus.

Procedures described by Mawlawi et al.(2001) were followed in defining the ventral striatum ROI. The dorsolateral boundary of the ventral striatum ROI, which separates it from the putamen and dorsal caudate, was defined in each coronal slice by "a line joining the intersection between the outer edge of the putamen with a vertical line going through the most superior and lateral point of the internal capsule and the center of the portion of the anterior commissure transaxial plane overlying the striatum. This line was extended to the internal edge of the caudate" (10). Marked image intensity differences allowed for the definition of the remaining boundaries in each coronal slice. The caudate defined the anterior extent of the ventral striatum ROI, and the anterior commissure in the coronal plane defined the posterior extent. Separate ROIs for the caudate and putamen contained all areas of these structures not included in the ventral striatum ROI. Different ROIs were also used for the anterior and posterior regions of the caudate and putamen, as defined by the anterior commissure.

The amygdala ROI was defined using a pre-rendered ROI mask available in AFNI. The mask was defined based on probability maps generated for various cortical areas (11) and the parcellation of cortical and subcortical structures generated by the FreeSurfer program using the "Talairach N27" atlas brain provided in AFNI. This map was altered to extend to the posterior edge of the amygdala as defined in the Mai atlas (Mai, et al., 2007).

The subgenual anterior cingulate cortex (ACC) was defined posteriorly by a line at the posterior border of the genu of the corpus callossum at the nadir of its concavity (y = 9) and anteriorly by a line at the anterior edge of the genu (y = 31) at the peak of its convexity. The medial and ventral boundaries of the ROI were defined by the medial and ventral surfaces of the cortex, respectively. The ROI extended dorsally to the fundus of the olfactory sulcus and the corpus callossum and laterally to the lateral edge of the olfactory sulcus.

The ventral pallidum ROI was defined anteriorly by the anterior commissure and extended 7 mm posterior from the commissure. The anterior commissure also defined the dorsal extent of the ventral pallidum, and ventrally the ROI included all of the subcommissural space (12). Based on the Mai atlas (Mai, et al., 2007) the ventral pallidum was defined laterally by a vertical line drawn 15 mm from the midline. It extended medially to a vertical line drawn 5 mm from the midline, which based on the Mai atlas appears to be the most lateral extent of the hypothalamus.

The insula region-of-interest masks were generated by FreeSurfer program, which we applied to the AFNI Talairach N27 atlas brain.

SUPPLEMENTAL RESULTS

Controlling for depression severity, anxiety severity, and anhedonia.

To determine whether between-appetite group differences in BOLD fMRI activity to food stimuli in the depressed patients remain after accounting for depression, anxiety, and anhedonia severity, we repeated the core ROI analyses described in the main text but this time controlled for illness severity factors. Within the seven ROI clusters identified in the HC subjects, we repeated the comparisons of the increase and decrease appetite depressed groups' responses to food pictures after covarying-out depression severity (as measured by the Hamilton Depression Rating Scale), anxiety severity (as measured by the Hamilton Anxiety Rating Scale), and the anhedonia (as measured by the Snaith-Hamilton Pleasure Scale). As can be seen in supplemental table S10, after covarying for these factors, the depressed subjects with appetite increases still exhibited greater activity than those with appetite decreases within the left OFC and bilateral mid-insula. Similarly, as seen in supplemental Table S11, controlling for depression, anxiety, and anhedonia did not substantially change the results of the whole-brain ANOVA (reported in Table S4) used to identify regions that exhibited group differences in responses to food images relative to non-food control images.

Effect of gender on responses to food images in increased and decreased appetite depressed subjects.

Another important area of future research will be to examine how appetite changes in depression interact with sex differences in responses to food cues. Several prior studies demonstrated sex differences to some food stimuli (13-15), and one study observed greater activity for women to high calorie foods in a region of the anterior insula observed here (15).

To address this, within the seven ROI clusters identified in the HC subjects, we repeated the comparisons of the increase and decrease appetite depressed groups' responses to food pictures separately for female and male subjects. Both male and female participants exhibited results that were generally qualitatively similar to the results for the entire sample. Qualitatively, both female and male depressed increase appetite subgroups exhibited greater responses to food pictures bilaterally in the insula (Table S13). In females considered alone,

the increased appetite depressed group exhibited greater responses in the left visual cortex ROI to food pictures than the decrease appetite group. Female increased appetite depressed subjects also exhibited greater responses than decreased appetite subjects in the left OFC. In males the responses of the two groups in the left OFC appeared nearly identical. Given the relatively small number of male subjects, however, this failure to observe a group difference in this ROI may reflect a limitation in statistical sensitivity.

No group differences in fMRI motion parameters.

No statistically significant differences were observed between the groups in average head motion during the fMRI scans (depressed decreased appetite Mean = .05mm (standard deviation = .03), depressed increased appetite Mean = .06mm (.02), healthy subject Mean = .05mm (.02)).

SUPPLEMENTAL DISCUSSION

Relationship to anhedonia

Clearly, the differential responses to food in the behavioral subgroups in the present study demonstrate that depression is not always associated with a global loss of interest in reward stimuli. The differences between the two groups of depressed subjects in putatively reward-related brain regions are striking specifically because the groups did not differ in overall levels of anhedonia (after excluding food-related items from the SHAPS anhedonia scale). One explanation for the potentiated activity to food cues in the appetite increase group may be that in this group the food reward dysfunction during depression reflects a relative imbalance between the hedonic versus the motivational aspects of reward (16). Such a phenomenon conceivably may result in increased salience for hedonically pleasing pictures, such as foods, concomitantly with a decrease in the motivational aspects of reward, as reflected by anhedonia ratings. If so, the increased appetite group may exhibit greater responses in these regions to reward cues generally, despite the persistence of anhedonia experientially. Nevertheless, it remains unclear whether the increased appetite group might exhibit increased reward circuitry responses to non-food rewards. Future research should seek to clarify this point.

Relationship to melancholic and atypical depression diagnostic specifiers

Recent latent class analyses of depressed cohorts have identified increases and decreases in appetite as the most discriminative symptoms among some depression subtypes. An older distinction exists however, that also bears mentioning in light of the present findings: the melancholic and atypical specifiers for a major depressive disorder diagnosis allowed in the Diagnostic and Statistical Manual (DSM). Melancholic depression is defined as a depression presenting with pervasive anhedonia or mood non-reactivity, as well as a combination at least three of the following: a negative distinct quality to mood, early morning wakening, excessive guilt, loss of appetite or weight, psychomotor agitation or retardation, and typically worse symptoms in the morning. In

contrast, atypical depression presents with mood reactivity and at least two of the following: increased appetite or hyperphagia, hypersomnia, leaden paralysis, and rejection sensitivity. Given our separation of the depressed subjects into those with increased and decreased appetite, it seems possible that the two groups in the present study might represent these atypical and melancholic subtypes. This appears to us to be unlikely however.

For example, atypical depression is usually associated with hypersomnia, and so we might expect the increased appetite depressed group to exhibit greater hypersomnia than the other group (17). In fact, however, the two depressed groups did not differ significantly in self-reported hypersomnia on the HDRS (see Table S12). Likewise, melancholic depression is hypothesized to be relatively more strongly associated with anxiety (18), yet the decreased appetite depressed group did not differ from the increased appetite depression group in anxiety as measured by either self-report or clinician interview (see Table 1). Nevertheless, some recent evidence may suggest that atypical and melancholic depression may be associated with differential hypothalamic-pituitary-adrenal axis function and inflammation (19), but see (20). As a result, these factors should be explored in future studies which compare subgroups of depressed subjects analogous to those studied here.

Implications for future research

A take-home message from the work described here appears to be that depression can have fairly variable behavioral presentations that are associated with different patterns of activity in reward and interoceptive neurocircuitry. To the extent that future researchers wish to compare depressed and healthy control subjects on tasks that assay activity in reward and interoceptive regions, it may be important to take into account heterogeneity in appetite changes among the depressed sample. Failure to do so may confound a study's results either by under- or over-estimating the effects of depression on reward and interoceptive tasks, depending on the particular sample of depressed subjects in the study

REFERENCES

1. Simmons WK, Rapuano KM, Kallman SJ, Ingeholm JE, Miller B, Gotts SJ, Avery JA, Hall KD, Martin A. Category-specific integration of homeostatic signals in caudal but not rostral human insula. Nat Neurosci. 2013;16:1551-1552.
2. Simmons WK, Rapuano KM, Ingeholm JE, Avery J, Kallman S, Hall KD, Martin A. The ventral pallidum and orbitofrontal cortex support food pleasantness inferences. Brain structure & function. 2014;219:473-483.
3. Jo HJ, Saad ZS, Simmons WK, Milbury LA, Cox RW. Mapping sources of correlation in resting state FMRI, with artifact detection and removal. Neuroimage. 2010;52:571-582.
4. Glover GH, Li TQ, Ress D. Image-based method for retrospective correction of physiological motion effects in fMRI: RETROICOR. Magn Reson Med. 2000;44:162-167.
5. Birn RM, Murphy K, Bandettini PA. The effect of respiration variations on independent component analysis results of resting state functional connectivity. Hum Brain Mapp. 2008;29:740-750.
6. Talairach J, Tournoux JTP: Co-planar Stereotaxic Atlas of the Human Brain. New York, NY, Thieme Medical Publishers; 1988.
7. van der Laan LN, de Ridder DT, Viergever MA, Smeets PA. The first taste is always with the eyes: a meta-analysis on the neural correlates of processing visual food cues. Neuroimage. 2011;55:296-303.
8. Rothemund Y, Preuschhof C, Bohner G, Bauknecht HC, Klingebiel R, Flor H, Klapp BF. Differential activation of the dorsal striatum by high-calorie visual food stimuli in obese individuals. Neuroimage. 2007;37:410-421.
9. Chiavaras MM, LeGoualher G, Evans A, Petrides M. Three-dimensional probabilistic atlas of the human orbitofrontal sulci in standardized stereotaxic space. Neuroimage. 2001;13:479-496.
10. Mawlawi O, Martinez D, Slifstein M, Broft A, Chatterjee R, Hwang DR, Huang Y, Simpson N, Ngo K, Van Heertum R, Laruelle M. Imaging human mesolimbic dopamine transmission with positron emission tomography: I. Accuracy and precision of D(2) receptor parameter measurements in ventral striatum. J Cereb Blood Flow Metab. 2001;21:1034-1057.
11. Desikan RS, Segonne F, Fischl B, Quinn BT, Dickerson BC, Blacker D, Buckner RL, Dale AM, Maguire RP, Hyman BT, Albert MS, Killiany RJ. An automated labeling system for subdividing the human cerebral cortex on MRI scans into gyral based regions of interest. Neuroimage. 2006;31:968-980.
12. Haber SN, Knutson B. The reward circuit: linking primate anatomy and human imaging. Neuropsychopharmacology. 2010;35:4-26.
13. Cornier MA, Salzberg AK, Endly DC, Bessesen DH, Tregellas JR. Sex-based differences in the behavioral and neuronal responses to food. Physiol Behav. 2010;99:538-543.
14. Frank S, Laharnar N, Kullmann S, Veit R, Canova C, Hegner YL, Fritsche A, Preissl H. Processing of food pictures: influence of hunger, gender and calorie content. Brain Res. 2010;1350:159-166.

15. Killgore WD, Yurgelun-Todd DA. Sex differences in cerebral responses to images of high versus low-calorie food. Neuroreport. 2010;21:354-358.
16. Treadway MT, Zald DH. Reconsidering anhedonia in depression: lessons from translational neuroscience. Neurosci Biobehav Rev. 2011;35:537-555.
17. Matza LS, Revicki DA, Davidson JR, Stewart JW. Depression with atypical features in the National Comorbidity Survey: classification, description, and consequences. Arch Gen Psychiatry. 2003;60:817-826.
18. Gold PW. The organization of the stress system and its dysregulation in depressive illness. Mol Psychiatry. 2014.
19. Lamers F, Vogelzangs N, Merikangas KR, de Jonge P, Beekman AT, Penninx BW. Evidence for a differential role of HPA-axis function, inflammation and metabolic syndrome in melancholic versus atypical depression. Mol Psychiatry. 2013;18:692-699.
20. Young EA, Carlson NE, Brown MB. Twenty-four-hour ACTH and cortisol pulsatility in depressed women. Neuropsychopharmacology. 2001;25:267-276.

Table S1. Regions exhibiting differences between food and non-food stimuli in healthy, non-depressed participants.

Side / Location	Peak Coordinates			T	Volume
	X	Y	Z		(mm^3)
Food > Non-food					
Right Visual Cortex	14.9	-85	-6.6	11.3	12256
Left Visual Cortex	-9.6	-85	-1.4	8.3	7528
Left Insula	-34.1	-8	14.4	6.1	1632
Left OFC	-23.6	32.2	-4.9	8.4	1296
Right Dorsal Mid-Insula	37.6	-6.2	9.1	8.2	920
Right Amygdala	18.4	0.8	-10.1	4.8	600
Right OFC	23.6	30.5	-4.9	3.8	208

All results corrected for multiple comparisons at $p < .05$

Table S2. Results of ROI analyses within regions from Table S1 for the two depressed groups.

Side / Location	Depressed-appetite increase		Depressed-appetite decrease		
	Mean	SD	Mean	SD	*p**
Right Visual Cortex	0.27	0.14	0.25	0.13	0.625
Left Visual Cortex	0.31	0.14	0.23	0.11	0.076
Left Insula	0.06	0.04	0.01	0.06	**0.010**
Left OFC	0.12	0.09	0.06	0.07	**0.046**
Right Dorsal Mid-Insula	0.06	0.05	0.01	0.05	**0.026**
Right Amygdala	0.06	0.06	0.04	0.07	0.507
Right OFC	0.08	0.07	0.04	0.08	0.170

* Independent samples t test

Regions highlighted in bold font exhibited statistically significant group differences.

Table S3. Effect size for regions from Table S1 exhibiting differences between food and non-food stimuli in HCs.

Regions	**Effect size**
Food > Non-food	**Depressed-increase vs Depressed-decrease**
Right Visual Cortex	0.174
Left Visual Cortex	0.660
Left Insula	0.992
Left OFC	0.741
Right Dorsal Mid-Insula	0.826
Right Amygdala	0.239
Right OFC	0.499

Cohen's d for independent t-test.

Table S4. Regions exhibiting Group (HC, Depressed-appetite increase, Depressed-appetite decrease) ANOVA main effects.

Side / Location	Peak Coordinates			F	Volume
	X	Y	Z		(mm^3)
Right Anterior Insula	+27	+22	-10	11.4	1456
Left Dorsal Mid-Insula	-31	-8	14	10.7	552
Right Ventral Pallidum	11	-1	-1	10.9	464
Right Ventral Striatum	20	11	-3	9.5	448
Left Ventral Striatum and Left OFC	-8	13	-5	8.9	416
Right OFC	13	48	-14	11.4	368
Right Dorsal Mid-Insula	40	-6	11	8.2	216
Left Anterior Insula	-29	27	0	6.7	168
Left Caudal Anterior Insula	-43	8	2	7.2	168
Right Putamen	31	3	2	8.3	96

All results corrected for multiple comparisons at $p < .05$

Table S5. Effect size for regions from Table S4 exhibiting group main effects in ANOVA.

Regions	Effect size		
	IN vs DE	IN vs HC	DE vs HC
Right Anterior Insula	1.583	0.883	-0.755
Left Dorsal Mid-Insula	1.547	0.372	-1.228
Right Ventral Pallidum	1.377	1.421	0.074
Right Ventral Striatum	1.363	1.190	-0.265
Left Ventral Striatum	1.186	1.441	0.241
Left vmPFC	1.281	1.546	-0.023
Right OFC	1.622	1.157	-0.400
Right Dorsal Mid-Insula	0.945	-0.477	-1.519
Left Anterior Insula	1.274	0.598	-0.836
Left Caudal Anterior Insula	1.180	-0.190	-1.138
Right Putamen	1.441	1.021	-0.352

Cohen's d for independent t-tests.
IN: Depressed-appetite increase group; DE: Depressed-appetite decrease group; HC: Healthy control group.

Table S6. Pleasantness ratings averaged across all food stimuli in the Food Pleasantness Task.

	Healthy Controls (N=14)		Depressed-appetite increase (N=16)		Depressed -appetite decrease (N=15)		*p*		
	Mean	SD	Mean	SD	Mean	SD	IN vs DE	IN vs HC	DE vs HC
All Food Pictures	3.68	0.49	4.38	0.87	3.39	0.85	0.004	0.011	0.275

Independent t-tests
IN: Depressed-appetite increase group; DE: Depressed-appetite decrease group; HC: Healthy control group.

Table S7. Pleasantness ratings separated by food category in the Food Pleasantness Task

	Healthy Controls (N=14)		Depressed-appetite increase (N=16)		Depressed-appetite decrease (N=15)		*p*		
	Mean	SD	Mean	SD	Mean	SD	IN vs DE	IN vs HC	DE vs HC
High Fat High Sweet	3.74	0.96	4.71	1.32	3.51	1.28	0.015	0.027	0.590
High Fat Low Sweet	3.91	1.16	5.12	0.95	3.67	1.14	0.001	0.004	0.589
Low Fat High Sweet	3.64	0.89	3.63	0.87	3.23	0.92	0.219	0.972	0.227
Low Fat Low Sweet	3.46	0.67	3.96	1.09	3.18	1.08	0.054	0.139	0.398

Independent t-tests
IN: Depressed-appetite increase group; DE: Depressed-appetite decrease group; HC: Healthy control group.

Table S8. Effect size for food pleasantness ratings

	Effect Size		
	IN vs DE	IN vs HC	DE vs HC
High Fat High Sweet	0.926	0.845	-0.203
High Fat Low Sweet	1.396	1.165	-0.204
Low Fat High Sweet	0.453	-0.013	-0.459
Low Fat Low Sweet	0.721	0.556	-0.423

Cohen's d for independent t-tests.
IN: Depressed-appetite increase group; DE: Depressed-appetite decrease group; HC: healthy control group.

Table S9. Regions exhibiting resting-state functional connectivity to the mid-insula seed regions that correlated with ratings of anticipated food pleasantness.

Seed Region	Side / Location	Peak Coordinates			T-score	Volume
		X	Y	Z		(mm^3)
Left Mid/Anterior Insula	Left ventral medial prefrontal cortex	-6.1	28.8	-4.9	3.63	160
Right Dorsal Mid-Insula	Left ventral medial prefrontal cortex	-7.9	30.5	-4.9	4.73	408
	Left ventral striatum	-7.9	4.2	-10.1	3.49	80

All results corrected for multiple comparisons at $p < .05$

Note: Seed regions defined by regions exhibiting differences between food and non-food stimuli in healthy, non-depressed participants (found in Supplemental Table S1). No other seed region (found in Table S1) exhibited reliable correlations with any other brain regions.

Table S10. Results of ROI analyses within regions from Table S2 for the two depressed groups *AFTER* controlling for depression, anxiety, and anhedonia severity.

Increase vs Decrease Appetite Depressed Groups	Original Analyses Without Covariates		Hamilton Anxiety Rating Scale Adjusted		Hamilton Depression Rating Scale Adjusted		Modified Snaith-Hamilton Pleasure Scale Adjusted	
	t	p	t	p	t	p	t	p
Right Visual Cortex	0.493	0.625	0.487	0.630	0.573	0.571	0.573	0.571
Left Visual Cortex	1.843	0.076	1.865	0.073	1.868	0.072	1.915	0.066
Left Insula	2.765	0.010	2.490	0.019	2.685	0.012	2.367	0.025
Left OFC	2.088	0.046	1.985	0.057	2.080	0.046	1.990	0.056
Right Dorsal Mid-Insula	2.337	0.026	2.109	0.043	2.236	0.033	2.175	0.038
Right Amygdala	0.672	0.507	0.369	0.715	0.528	0.601	0.672	0.507
Right OFC	1.408	0.170	1.317	0.198	1.477	0.150	1.223	0.231

Regions highlighted in bold font exhibited statistically significant group differences.

Table S11. Results of ROI analyses within regions from Table S3 for the two depressed groups *AFTER* controlling for depression, anxiety, and anhedonia severity.

Increase vs Decrease Appetite Depressed Groups	Original Analyses Without Covariates		Hamilton Anxiety Rating Scale Adjusted		Hamilton Depression Rating Scale Adjusted		Modified Snaith-Hamilton Pleasure Scale Adjusted	
	t	p	t	p	t	p	t	p
Right Anterior Insula	4.4608	0.0001	4.2741	0.0002	4.4502	0.0001	3.9262	0.0005
Left Dorsal Mid-Insula	4.3512	0.0002	4.0641	0.0003	4.2359	0.0002	3.9080	0.0005
Right Ventral Pallidum	3.7993	0.0008	3.6293	0.0013	3.7357	0.0010	3.3436	0.0024
Right Ventral Striatum	3.8541	0.0006	3.6471	0.0010	3.8444	0.0006	3.2834	0.0026
Right OFC	4.5870	0.0001	4.8577	0.0000	4.5709	0.0001	4.0218	0.0004
Right Dorsal Mid-Insula	2.6677	0.0123	2.4222	0.0219	2.5501	0.0162	2.5535	0.0161
Left Anterior Insula	3.5989	0.0011	3.4525	0.0017	3.7017	0.0009	3.2448	0.0029
Left Caudal Ant. Insula	3.2482	0.0033	2.9747	0.0063	3.1306	0.0044	2.8752	0.0079
Right Anterior Putamen	4.0696	0.0003	4.0836	0.0003	4.3529	0.0001	3.3315	0.0023
Left Ventral Striatum	3.3539	0.0022	3.2103	0.0032	3.3067	0.0025	2.9800	0.0057
Left vmPFC	3.5902	0.0012	3.4751	0.0017	3.6216	0.0012	3.0026	0.0057

Regions highlighted in bold font exhibited statistically significant group differences.

Table S12. Sleep Questions from the Hamilton Depression Rating Scale

	Depressed-appetite increase (N=16)		Depressed-appetite decrease (N=16)			
	Mean	SD	Mean	SD	t-statistic	*p*
Sleep Onset (item H6)	1.1	1.0	1.0	1.0	0.37	.72
Sleep Maintenance (item H7)	1.2	0.7	1.3	0.9	0.23	.82
Early Awakening (item H8)	0.3	0.7	0.0	0.0	1.78	.10
Hypersomnia (item A6)	0.3	0.7	0.3	1.0	0.20	.84

Table S13. Results of ROI analyses within regions from Table S1 for the two depressed groups separately for Female and Male participants.

Side / Location	FEMALE Depressed-appetite increase		FEMALE Depressed-appetite decrease		
	Mean	SD	Mean	SD	*p**
Right Visual Cortex	0.30	0.14	0.23	0.13	0.27
Left Visual Cortex	0.34	0.13	0.23	0.09	**0.02**
Left Insula	0.06	0.05	0.02	0.04	**0.05**
Left OFC	0.13	0.09	0.06	0.07	**0.04**
Right Dorsal Mid-Insula	0.05	0.05	0.01	0.05	**0.05**
Right Amygdala	0.06	0.06	0.06	0.06	0.84
Right OFC	0.09	0.07	0.05	0.08	0.22

Side / Location	MALE Depressed-appetite increase		MALE Depressed-appetite decrease		
	Mean	SD	Mean	SD	*p**
Right Visual Cortex	0.16	0.08	0.27	0.13	0.23
Left Visual Cortex	0.18	0.13	0.24	0.14	0.60
Left Insula	0.07	0.02	-0.01	0.08	0.18
Left OFC	0.05	0.02	0.06	0.09	0.90
Right Dorsal Mid-Insula	0.07	0.05	0.02	0.07	0.25
Right Amygdala	0.03	0.04	0.00	0.07	0.45
Right OFC	0.03	0.05	0.03	0.08	0.93

* Independent samples t test
Regions highlighted in bold font exhibited statistically significant group differences.

Figure S1. Schematic depiction of the Food/Non-food Picture Task. Participants saw photographs of food and non-food objects for 2.5 seconds each, and pressed a button anytime they saw the same basic-level object presented twice in a row. Reprinted from Simmons et al. (2012) with permission from the Nature Publishing Group.

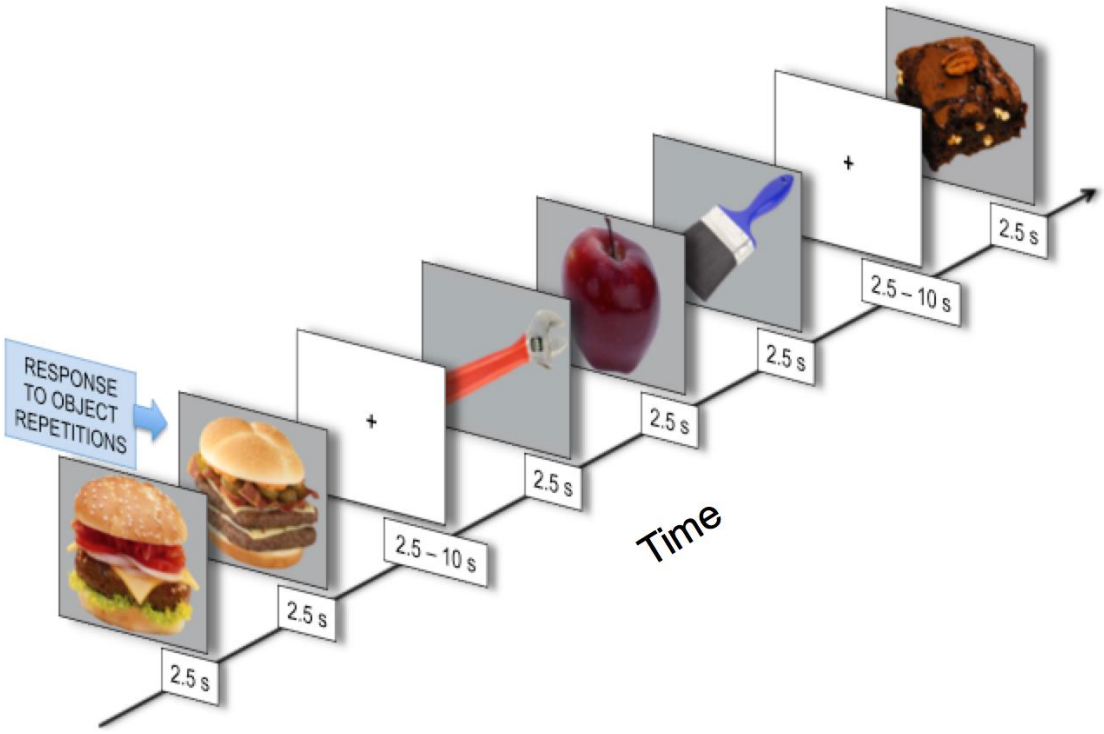

Figure S2. Example Stimuli presented in the Food Pleasantness Task. On the same day they performed the Food/non-food Picture Task, the subjects also performed a Food Pleasantness Task in which they rated how pleasant it would be at that moment to eat foods depicted in photographs drawn from a well-controlled corpus of food images. The photographs depicted items from four classes of foods that were validated in a prior study in healthy adults (2).

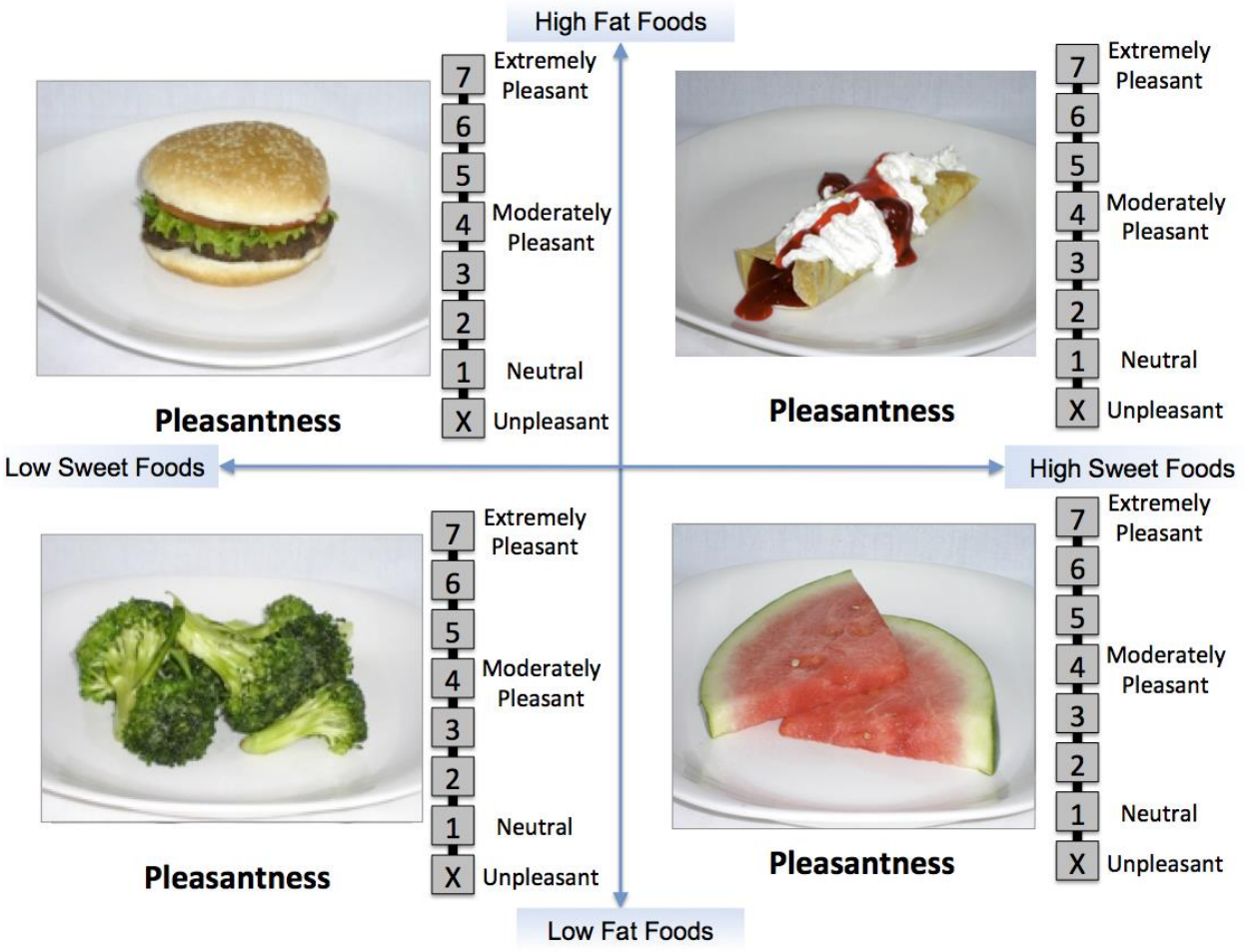

Figure S3. Ratings on the Food Pleasantness Task. Depressed subjects with increased appetite provided higher inferred pleasantness ratings than both of the other groups for both high-fat high sweet foods and high-fat low-sweet foods, with a trend toward higher ratings for low-fat low-sweet foods in comparison to the depressed group with appetite.

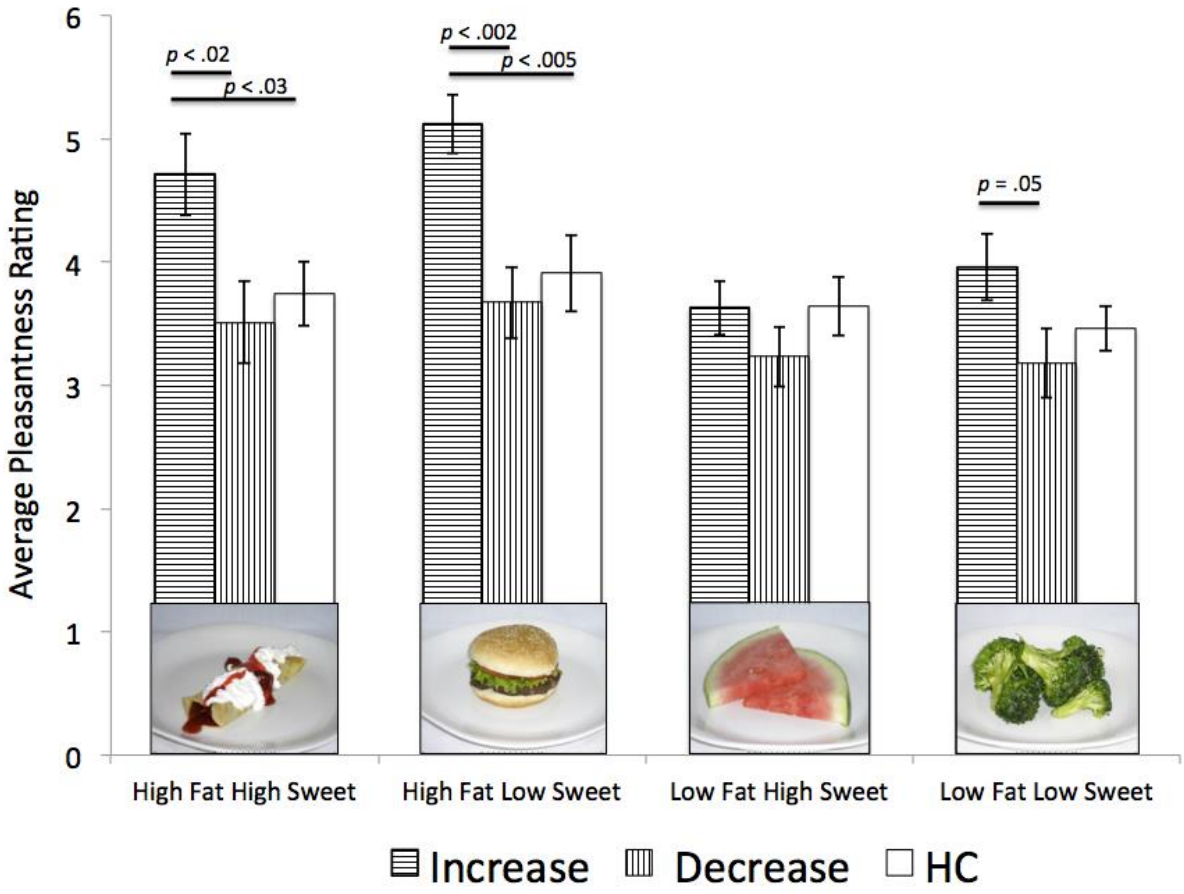

Figure S4. Average temporal signal-to-noise (TSNR) map for fMRI data
These maps show the average TSNR of the smoothed echo-planar imaging (EPI) time course data. TSNR was calculated by dividing each voxel's mean signal intensity by the standard deviation of the time-course. All colored areas shown have TSNR of at least 40, the minimum to reliably detect effects between conditions in fMRI data (7). All areas in red have a TSNR of at least 150.